of the boundary value problem is easy to survey. The eigenvalues calculated directly from (15) can be coordinated to the individual modes of the fin line. The method converges very rapidly and the calculated results for realistic models are in good agreement with experimental results.

REFERENCES

[1] A. Farrar and A. T. Adams, "Characteristic impedance of microstrip by the method of moments," *IEEE Trans. Microwave Theory Tech.*, vol. MTT-18, pp. 65–66, 1970.
[2] W. J. R. Hoefer and A. Ros, "Fin line parameters calculated with the TLM-method," in *1979 IEEE MTT-S Intern. Microwave Symp. Dig.* (Orlando, FL), pp. 341–343.
[3] H. Hofmann, "Dispersion of planar waveguides for millimeter-wave application," *Arch. Elektron. Übertragung.*, vol. 31, pp. 40–44, 1977
[4] P. J. Meier, "Equivalent relative permittivity and unloaded Q factor of integrated fin-line," *Electron. Lett.*, vol. 9, pp. 162–163, 1973.
[5] ——, "Integrated fin-line millimeter components," *IEEE Trans. Microwave Theory Tech.*, vol. MTT-22, pp. 1209–1216, 1974.
[6] J. P. Montgomery, "On the complete eigenvalue solution of ridged waveguide," *IEEE Trans. Microwave Theory Tech.*, vol. MTT-19, pp. 547–555, 1971.
[7] A. M. K. Saad and G. Begemann, "Electrical performance of fin lines of various configurations," *Inst. Elec Eng. J. Microwaves, Opt., Acoust (MOA)*, vol. 1, pp. 81–88, 1977.
[8] A. M. K. Saad and K. Schünemann, "A simple method for analyzing fin line structures," *IEEE Trans. Microwave Theory Tech.*, vol. MTT-26, pp. 1002–1007, 1978.

Microstrip Spiral Directional Coupler

KOJI SHIBATA, KOZO HATORI, SENIOR MEMBER, IEEE, YASUYUKI TOKUMITSU, MEMBER, IEEE, AND HIDEMITSU KOMIZO, MEMBER, IEEE

Abstract—**A new microwave directional coupler with a spiral-shaped construction is described. This coupler is named the spiral coupler and is formed by coiling two edge-coupled lines. Therefore, the size of the coupler can be greatly miniaturized. Furthermore, this coupler can achieve tight coupling much easier than the conventional coupler with edge-coupled lines on account of the multiconductor structure. The spiral couplers with a total length of a quarter-wave were fabricated on alumina ceramic substrates and resulted in 3.5-dB maximum coupling for a 40-μm strip spacing. The size of the coupler was about one-sixth of the conventional one. The spiral coupler with a total length of three quarter-waves theoretically showed 2.5-dB coupling for a 95-μm strip spacing on an alumina substrate. The achieved coupling is due to the skillful construction of the spiral. An experimental coupler fabricated on a Teflon substrate confirmed the usefulness of this approach.**

I. INTRODUCTION

AS THE SIZE of microwave integrated circuit has become much smaller in recent years, a small-sized directional coupler, especially, a wide-band 3-dB hybrid is often required. In the microwave integrated circuitry, interdigitated microstrip couplers have been developed [1], [2] since the first description by Lange [3]. But these couplers are a quarter-wave length for a single section and a much longer length for multisection couplers.

In order to obtain the small-sized directional coupler with tight coupling in wide strip spacings, a new microwave directional coupler with a spiral-shaped construction is proposed in this paper and we have named it a "spiral coupler."

The spiral coupler is formed by coiling two edge-coupled lines and is shown in Fig. 1(a), (b) as type-*A* coupler. Consequently, the size of the coupler is miniaturized. Furthermore, this coupler can achieve tight coupling much easier than the conventional coupler with edge-coupled lines, because the recoupled power which is a portion of the transmitted power increases the degree of coupling on account of the multiconductor structure.

In this paper, we describe the theoretical and experimental results and show good agreement between these results.

In the theoretical analysis, we have derived the relation between the dimensions of microstrip conductors and the circuit parameters of multiconductor transmission lines. Using these results, the performance of the coupler is calculated. In the experimental results, we show the perfor-

Manuscript received October 13, 1980; revised January 6, 1981. A condensed version of this paper has been presented at the 1980 IEEE-MTTS International Microwave Symposium, Washington, DC.

K. Shibata is with the Kitami Institute of Technology, Kitami, 090 Japan.
K. Hatori is with the Research Institute of Applied Electricity, Hokkaido University, Sapporo, 060 Japan.
Y. Tokumitsu and H. Komizo are with Fujitsu Laboratories Ltd., Kawasaki, 211 Japan.

0018-9480/81/0700-0680$00.75 ©1981 IEEE

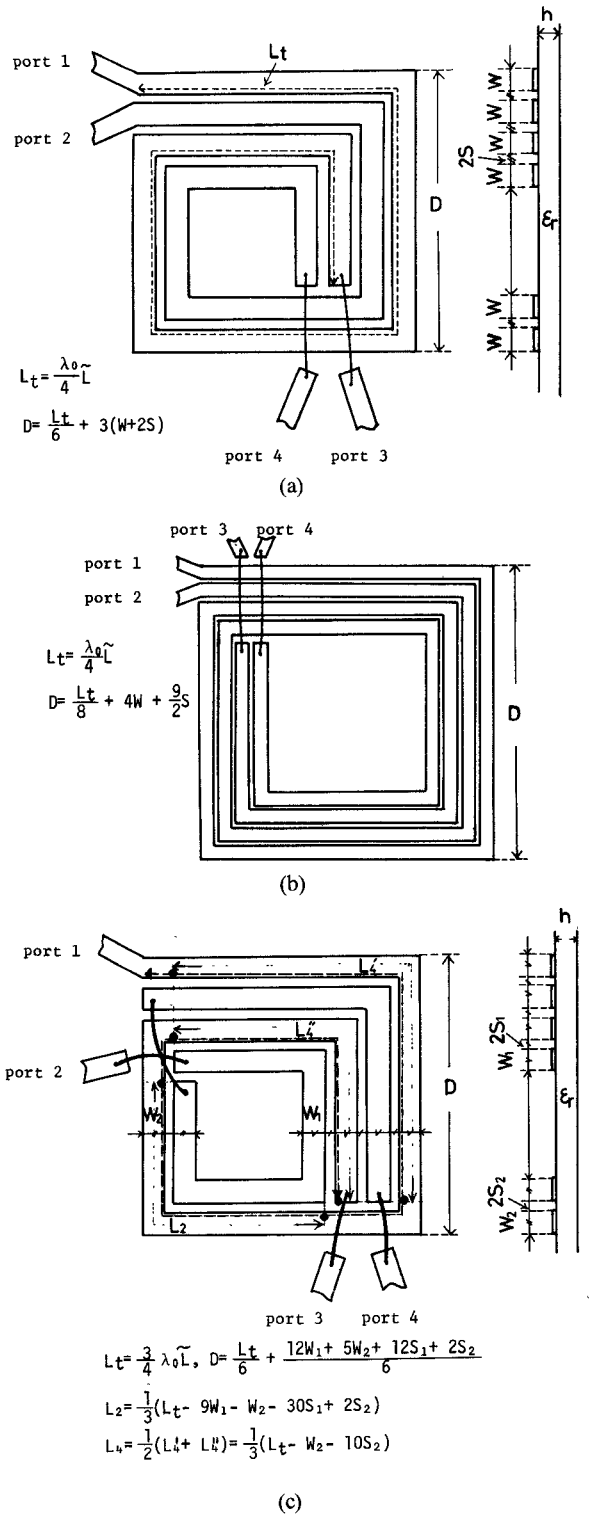

Fig. 1. Construction of spiral couplers. (a) Type-*A* coupler (1.5-turn spiral). (b) Type-*A* coupler (2-turn spiral). (c) Type-*B* coupler.

mances of the spiral couplers with 1.5- and 2-turn rectangular spirals on alumina ceramic substrates, which are named type-*A* couplers. For both couplers, 3.5-dB maximum coupling was obtained for a 40-μm strip spacing. The spacing is ten times as wide as that of the conventional edge-coupled directional coupler and the spiral coupler uses much smaller area of substrate than the conventional coupler. We show another type of a spiral coupler, which is named type-*B* coupler, in Fig. 1(c). The total length of this coupler is three quarter-waves. This coupler corresponds to the conventional coupler with three-section coupled transmission lines. We show design examples and experimental results of the trial construction. Type-*A* coupler can be used in the frequency range below 3 GHz, because a side length of the spiral should be long enough for fabrication. For the same reason, type-*B* coupler can be used in the frequency range up to *X*-band.

II. Theoretical Analysis and Design

A. General Remarks

The spiral couplers are considered as cascades of multiconductor coupled-line sections. While the alternate lines are of equal potential in the interdigitated coupler, the concept is not applicable to analysis of the spiral coupler. So, a separate analysis must be made.

The four-port circuits which are equivalent to the spiral couplers are shown in Fig. 2. In the analysis, the coupled lines are assumed to be ideally connected. Therefore, analysis of the spiral coupler is reduced to that of multiconductor transmission lines. The number of lines is limited to less than or equal to four, because 3-dB coupling is realizable with a 1.5–2-turn spiral. We assume equal strip width and spacing on the multiconductor structure for simplicity.

The outline of our analysis is described as follows. If we know the relation between the dimensions of strips and the capacitance parameters, a scattering matrix $\boldsymbol{S}$, which conveniently describes the coupler performance, can readily be obtained. Therefore, in the first place, we calculate the capacitance parameters by making use of the spectral-domain method reported in a recent paper [4], because this method is appropriate for capacitance calculation of multiconductor printed lines. Then, we derive the admittance parameters, from which the scattering parameters are obtained. In this calculation, we derive the admittance matrix ($\boldsymbol{Y}$) of a symmetrical four-line microstrip in terms of the self- and mutual admittances, because matrix $\boldsymbol{Y}$ has not been derived in an explicit form.

B. Capacitance Calculation

The coupling section of four lines under analysis is shown in Fig. 3. For computation of the capacitances, we assume the TEM mode for wave propagation.

With regard to a four-line microstrip structure, the capacitance matrix element C_{ij} is equal to C_{ji} because of the symmetric structure. The assumption $C_{13}=C_{14}=0$ may be assumed in almost all practical cases. In obtaining the capacitance matrix, it is convenient to use the capacitances for even- and odd-mode excitation. The even-mode excitation occurs when all conductors are held at the same potential; the odd-mode excitation occurs when the succeeding adjacent conductors are held at opposite polarity potentials of equal magnitude. Therefore, C_{ij} is expressed

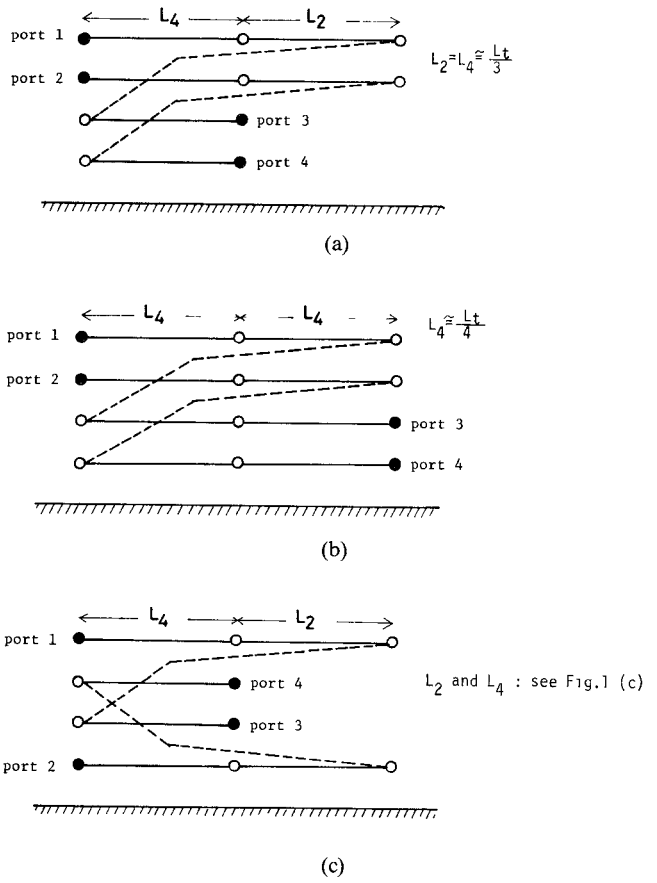

Fig. 2. Equivalent circuits of spiral couplers. (a) Type-*A* coupler (1.5-turn spiral). (b) Type-*A* coupler (2-turn spiral). (c) Type-*B* coupler.---denotes that the points are identical.

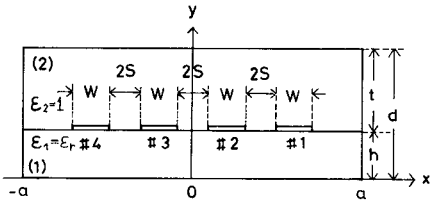

Fig. 3. Model for calculation of capacitance matrix of four-line microstrip.

in terms of the even- and odd-mode capacitances C_e^i, C_o^i (strip number: $i=1,2$) as follows:

$$C_{11}=(C_e^1+C_o^1)/2$$
$$C_{22}=(C_e^2+C_o^2)/2$$
$$C_{12}=(C_e^1-C_o^1)/2$$
$$C_{23}=-(C_e^1-C_o^1)/2+(C_e^2-C_o^2)/2. \quad (1)$$

These capacitances are calculated for the vacuum- and the dielectric-filled cases. The thickness of the strips is assumed to be negligible. In Fig. 3, $t/h=a/h=50$ is assumed throughout the calculation in order to avoid the influence of the upper and side walls on the capacitance values. The same procedure as in [4] is used. The unknown charge distribution function $\rho_s(x)$ on the sth strip is expressed in terms of known basis functions $\rho_p^s(x)$

$$\rho_s(x)=\sum_{p=1}^{N} c_p^s \rho_p^s(x). \quad (2)$$

The following linear equations for unknown coefficients c_p^s are obtained:

$$\sum_{s=1}^{2}\sum_{p=1}^{N} c_p^s X_{pj}^{sm}=\frac{a}{2}V_m \qquad (j=1,2,\cdots,N;\ m=1,2) \quad (3)$$

$$X_{pj}^{sm}=\sum_{n=1}^{\infty}\tilde{\rho}_p^s(n)\tilde{G}(n)\tilde{\rho}_j^m(n) \quad (4)$$

where $\tilde{\rho}_p^s(n)$ is finite Fourier transform [4] of the assumed charge distribution $\rho_p^s(x)$, V_m is the potential on the mth

TABLE I
COMPARISON OF OUR RESULTS FOR FOUR-LINE MICROSTRIP WITH PUBLISHED DATA

	Dimensions(mm)	Coupling	
Reference[3] (J.Lange)	h=1.0668 W=0.1143 2S=0.0762	(experiments) 3 dB	(calculation in this paper) 2.914 dB
Reference[5] (D.D.Paolino)	h=0.635 W=0.0711 2S=0.0508	(calculation) 3.0589 dB	(calculation in this paper) 3.0629 dB

strip, and $\tilde{G}(n)$ is expressed in (5)

$$\tilde{G}(n)=1/\epsilon_0\hat{k}_n\left[\epsilon_1\coth\left(\hat{k}_n h\right)+\epsilon_2\coth\left(\hat{k}_n t\right)\right]$$
$$\hat{k}_n=(2n-1)\pi/2a \quad \text{(for the even mode)}$$
$$\hat{k}_n=n\pi/a \quad \text{(for the odd mode).} \tag{5}$$

c_p^s is calculated by solving the simultaneous equations (3) by setting $V_1=V_2=1$ in the even-mode case and $V_1=-V_2=1$ in the odd-mode case. The line capacitance per unit length of the sth strip C_s is given by (6)

$$C_s=\sum_{p=1}^{N} c_p^s. \tag{6}$$

Preliminary computation showed the following basis functions were suitable for this multiconductor structure and that the number of basis functions (N) for accurate calculation was 2, that is, the matrix size was (4×4)

$$\rho_1^1(x)=\frac{1}{\pi\sqrt{\left(\frac{W}{2}\right)^2-\left(x-3S-\frac{3}{2}W\right)^2}}$$
$$\rho_2^1(x)=\frac{4}{5W}\left\{1+\left|\frac{2\left(x-3S-\frac{3}{2}W\right)}{W}\right|^3\right\}$$
$$\rho_1^2(x)=\frac{1}{\pi\sqrt{\left(\frac{W}{2}\right)^2-\left(x-S-\frac{W}{2}\right)^2}}$$
$$\rho_2^2(x)=\frac{4}{5W}\left\{1+\left|\frac{2\left(x-S-\frac{W}{2}\right)}{W}\right|^3\right\}. \tag{7}$$

We checked the accuracy of our calculation by comparing our results for a four-line microstrip with published data, which are described in [3], [5]. The comparison is shown in Table I. The capacitances of two coupled lines can be obtained in a similar manner. We ascertained a good agreement of our results with those reported in [6].

C. Admittance Parameters

The Y-matrix of the coupler ($\tilde{\boldsymbol{Y}}$) can be obtained from that of the coupled four lines ($\boldsymbol{Y}$) and the chain matrix of two coupled lines ($\boldsymbol{C}_m$) or only from the matrix $\boldsymbol{Y}$, by imposing the terminal conditions that the currents and voltages continue at the points where the lines are connected. When the spiral coupler is made up of two and four coupled lines in type-A coupler, the matrix $\tilde{\boldsymbol{Y}}$ is expressed in (8). In other cases, the matrices are derived in Appendix I

$$\tilde{\boldsymbol{Y}}=\boldsymbol{y}_3+\boldsymbol{y}_4(\boldsymbol{A}-\boldsymbol{y}_1)^{-1}\boldsymbol{y}_2 \tag{8}$$

where $\boldsymbol{y}_1\sim\boldsymbol{y}_4$ and $\boldsymbol{A}$ are expressed as follows:

$$\boldsymbol{Y}=\left[Y_{ij}\right] \qquad \boldsymbol{C}_m=\begin{bmatrix}\boldsymbol{a} & \boldsymbol{b}\\ \boldsymbol{c} & \boldsymbol{a}\end{bmatrix} \tag{9a}$$

$$\boldsymbol{y}_1=\left[\begin{array}{cc:cc} Y_{22} & Y_{12} & Y_{17} & Y_{27}\\ Y_{12} & Y_{11} & Y_{18} & Y_{17}\\ \hdashline Y_{17} & Y_{18} & Y_{11} & Y_{12}\\ Y_{27} & Y_{17} & Y_{12} & Y_{22}\end{array}\right]=\left[\begin{array}{c:c} y_1^{11} & y_1^{12}\\ \hdashline y_1^{21} & y_1^{22}\end{array}\right]$$

$$\boldsymbol{y}_2=\left[\begin{array}{cc:cc} Y_{13} & Y_{23} & Y_{26} & Y_{16}\\ Y_{14} & Y_{13} & Y_{16} & Y_{15}\\ \hdashline Y_{15} & Y_{16} & Y_{13} & Y_{14}\\ Y_{16} & Y_{26} & Y_{23} & Y_{13}\end{array}\right]$$

$$\boldsymbol{y}_3=\left[\begin{array}{c:c} y_1^{22} & y_1^{21}\\ \hdashline y_1^{12} & y_1^{11}\end{array}\right]$$

$$\boldsymbol{y}_4=\boldsymbol{y}_2' \tag{9b}$$

$$\boldsymbol{A}=\left[\begin{array}{c:c} -\boldsymbol{b}^{-1}\boldsymbol{a} & \boldsymbol{b}^{-1}\\ \hdashline -\boldsymbol{c}+\boldsymbol{a}\boldsymbol{b}^{-1}\boldsymbol{a} & -\boldsymbol{a}\boldsymbol{b}^{-1}\end{array}\right]. \tag{9c}$$

Matrix $\boldsymbol{Y}$ can be derived, as shown in Appendix I, from the capacitance matrix of the four-line microstrip that was calculated in the previous section and $\boldsymbol{C}_m$ [7] from the even- and odd-mode capacitances.

D. Calculation of Coupler Performance

The scattering parameters are expressed in terms of the matrix $\tilde{\boldsymbol{Y}}$ on the assumption that all the ports of the coupler are connected to lines with a characteristic impedance $Z_l(=50\ \Omega)$

$$\boldsymbol{S}=\boldsymbol{Z}_l^{1/2}\left(\boldsymbol{Y}_l-\tilde{\boldsymbol{Y}}\right)\left(\boldsymbol{Y}_l+\tilde{\boldsymbol{Y}}\right)^{-1}\boldsymbol{Z}_l^{-1/2} \tag{10}$$

where $\boldsymbol{Z}_l(=\boldsymbol{Y}_l^{-1})=Z_l\boldsymbol{1}_4$ is the load impedance matrix, $\boldsymbol{Z}_l^{1/2}$ is the square root matrix of $\boldsymbol{Z}_l$, and $\boldsymbol{1}_4$ is a unit matrix. From (10), the design charts can be drawn. In Fig.

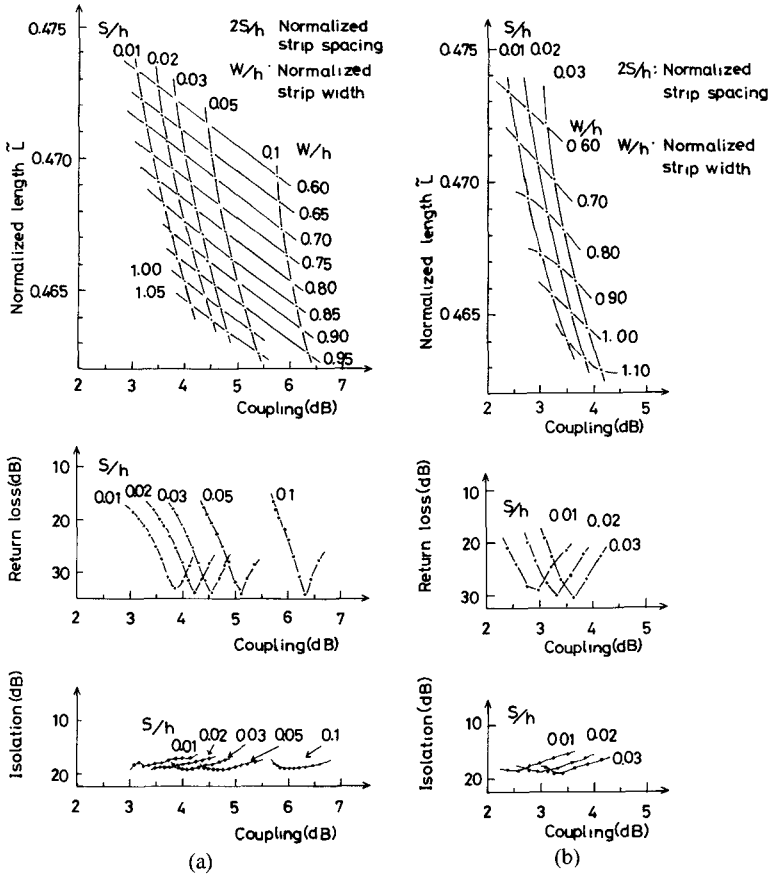

Fig. 4. Design charts of spiral couplers on an alumina substrate ($\epsilon_r = 9.6$). (a) Type-*A* coupler (1.5-turn spiral). (b) Type-*A* coupler (2-turn spiral).

TABLE II
DESIGN EXAMPLES OF TYPE-*B* COUPLER ON AN ALUMINA SUBSTRATE $\epsilon_r = 9.6$

	Spacing (mm)		Strip width(mm)		Total length				Coupling	Direct
	$2S_1$	$2S_2$	W_1	W_2	L_t (mm)	D (mm)	h (mm)	f_0 (GHz)	(dB)	(dB)
(i)	0.095	0.095	0.419	0.673	33.46	7.09	0.635	3	-2.51	-3.59
(ii)	0.127	0.064	0.476	0.667	33.34	7.20	0.635	3	-2.70	-3.36
(iii)	0.190	0.064	0.540	0.667	34.70	7.62	0.635	3	-3.42	-2.67
(i)'	0.045	0.045	0.198	0.318	16.73	3.50	0.3	6	-2.51	-3.59
(ii)'	0.060	0.030	0.225	0.315	16.67	3.56	0.3	6	-2.70	-3.36
(iii)'	0.090	0.030	0.255	0.315	17.35	3.76	0.3	6	-3.42	-2.67

Dimensions Normalized by the Thickness of the Substrate

	S_1/h	S_2/h	W_1/h	W_2/h
(i),(i)'	0.075	0.075	0.66	1.06
(ii),(ii)'	0.10	0.05	0.75	1.05
(iii),(iii)'	0.15	0.05	0.85	1.05

4 and Table II, we show the design charts for type-*A* coupler and design examples of type-*B* coupler. In the design examples of type-*B* coupler, we took given strip spacings ($2S_1, 2S_2$) and optimized W_1, W_2 in such a way that the reflected and isolated signals were minimized. An example of the theoretical performance of type-*B* coupler is shown in Fig. 5. From the charts, we can see the coupler dimensions, that is, strip spacing, width for necessary coupling, and coupler length corresponding to the prescribed center frequency. $\tilde{L}$ in the charts is the coupler length normalized with free-space wavelength λ_0 at a given center frequency f_0, so the charts are center-frequency independent. Total length L_t is expressed in (11)

$$L_t = \frac{\lambda_0}{4}\tilde{L}; \quad \tilde{L} = \bar{\lambda}_g(1+\tilde{\delta}_1) \qquad \text{(for type-}A\text{ coupler)} \tag{11a}$$

$$L_t = \tfrac{3}{4}\lambda_0\tilde{L}; \quad \tilde{L} = \bar{\lambda}_g(1+\tilde{\delta}_2) \qquad \text{(for type-}B\text{ coupler).} \tag{11b}$$

$\bar{\lambda}_g$ is the mean wavelength of normal modes on multicon-

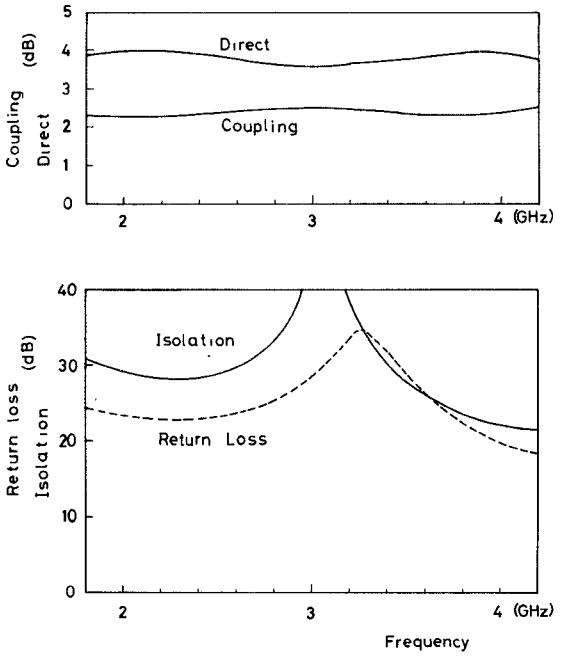

Fig. 5. Calculated performance for type-*B* coupler versus frequency with parameters as given in Table II. (Strip spacing $2S_1 = 2S_2 = 95\ \mu$m).

TABLE III
DESIGN PARAMETERS OF SPIRAL COUPLERS FOR TRIAL CONSTRUCTION

(I) Type A coupler on an alumina substrate (h=0.635 mm, ε_r=9.6)

		2S(mm)	W(mm)	L_t(mm)	D(mm)	f_0(MHz)	Coupling(dB) (at f=f_0)
1.5 turn	#1	0.040	0.395	48.51	9.44	750	3.88
	#2	0.063	0.454	48.37	9.65	750	4.57
2 turn	#3	0.043	0.427	48.43	7.99	780	3.32

(II) Type B coupler on a Teflon substrate (h=0.80 mm, ε_r=2.7)

2S(mm)	W(mm)	L_t(mm)	D(mm)	f_0(GHz)
0.20	0.90	90.0	18.0	2.0

ductor lines, which is normalized with λ_0, and is given in (12)

$$\bar{\lambda}_g = \frac{1}{6}\left[\frac{1}{\sqrt{x_1^a}} + \frac{1}{\sqrt{x_1^b}} + \frac{1}{\sqrt{x_2^c}} + \frac{1}{\sqrt{x_2^d}} + \frac{\lambda_{ge}}{\lambda_0} + \frac{\lambda_{go}}{\lambda_0}\right] \tag{12a}$$

$$\bar{\lambda}_g = \frac{1}{4}\left[\frac{1}{\sqrt{x_1^a}} + \frac{1}{\sqrt{x_1^b}} + \frac{1}{\sqrt{x_2^c}} + \frac{1}{\sqrt{x_2^d}}\right]. \tag{12b}$$

Taking the coupler length in (11), we calculated the scattering parameters and determined the optimum $\tilde{\delta}_1$, $\tilde{\delta}_2$ so that maximum coupling might be obtained at the center frequency. Using the optimum $\tilde{\delta}_1$, $\tilde{\delta}_2$, the coupler length is calculated by (11) and is described in Fig. 4 and Table II. The formula (12b) is applied to the case where the spiral coupler is made up of four lines only.

[1]Nomenclature as in Appendix II.

E. Design

Using the design charts in Fig. 4, we constructed several couplers of type-*A* with rectangular spirals on alumina ceramic substrates. Circular spiral is also applicable to construction of the spiral couplers. The dimensions of fabricated couplers of type-*A* are shown in Table III. Type-*B* coupler for trial construction was built on a Teflon substrate, whose dimensions are also shown in Table III.

III. EXPERIMENTS

Several couplers of type-*A* were built on alumina ceramic substrates of 0.635-mm thickness. The dielectric permittivity (ϵ_r) was 9.6. The thickness of the gold layer was 5 μm. The midband couplings were 3–4 dB. The photograph of 1.5-turn spiral coupler (#1) is shown in Fig. 6. The measured characteristics of scattering parameters and calculated responses are shown in Fig. 7. (a) and (b). The test data on these couplers show that the return losses are more than 20 dB, 25 dB, respectively, for a 1.5-turn coupler over an octave band and more than 19 dB for a 2-turn coupler.

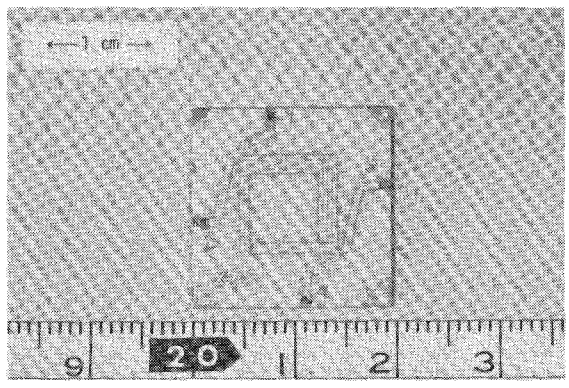

Fig. 6. Photograph of type-A coupler with 1.5-turn spiral (#1).

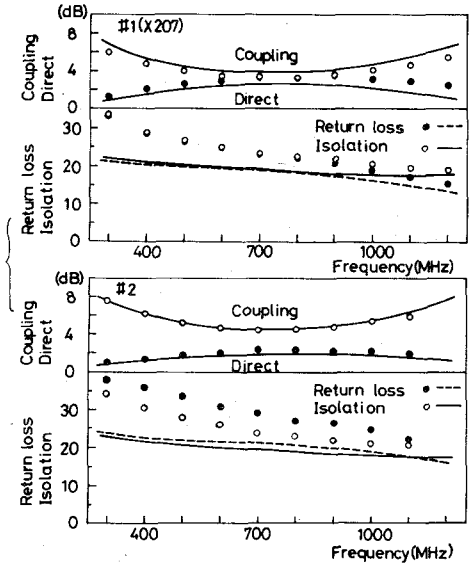

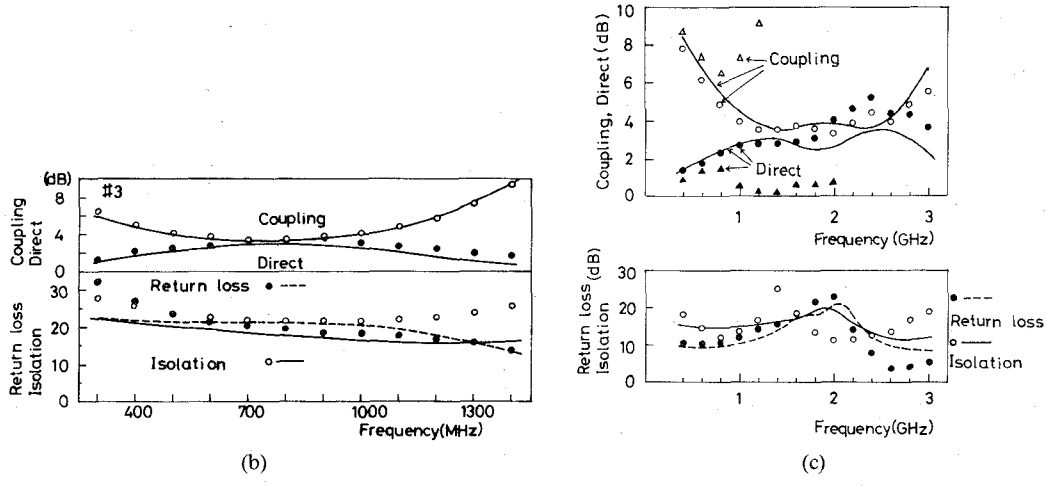

Fig. 7. Test data (dots) of spiral couplers (calculated data; solid and dotted lines). (a) Type-A couplers (1.5-turn spiral). (b) Type-A coupler (2-turn spiral). (c) ●○: type-B coupler. ▲△: type-A coupler with the same dimensions as those of type-B coupler.

The isolation is more than 21 dB for both 1.5-turn couplers and more than 22 dB for the 2-turn coupler, over the same band. The couplings at the center frequency agree well with the calculated values, which are listed in Table III, being within 0.38 dB(#1), 0.13 dB(#2), and 0.27 dB(#3). The frequency characteristics of coupling also agree well with the calculated ones being within a maximum discrepancy of 0.50 dB(#1), 0.15 dB(#2), and 0.32 dB(#3) over the same band.

The phase difference of coupled and transmitted waves

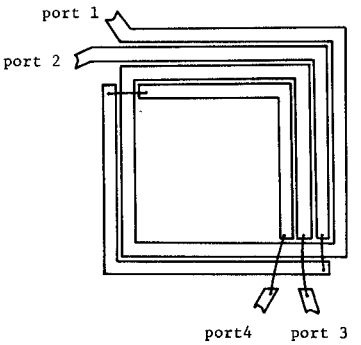

Fig. 8. Correction method of the difference of line length in inner side and that of outer side.

was tested on the #1 coupler which has about 3-dB coupling. The deviation of phase difference from 90° was ±3° over the same octave band. The measured responses of type-*B* coupler are shown in Fig. 7(c), in which are also depicted the responses of type-*A* coupler with the same dimensions as the type-*B* coupler. By making use of the method of constructing a type-*B* coupler, the center frequency shifted from 800 MHz to 2.0 GHz and the coupling of 6.5 dB in type-*A* coupler became 3.5 dB.

Therefore, a small-sized coupler with tight coupling can be successfully constructed with very wide strip spacing. In addition, a broad band of operation can be expected because the structure is equivalent to a three-section coupler.

IV. Discussion

The discrepancy between theoretical and measured responses of return loss and isolation can be attributed to wire-bond effects, line losses, and corner effects, none of which were computer programmed. The influence of the corner in rectangular spiral on coupler performances will disappear if we adopt the circular form of the spiral. Therefore, the problem of corner effects is not inherent in the spiral coupler. To a first approximation, the difference of line length between the inner and outer side of a spiral may be neglected, because the phase difference of two output waves was 90°±3° for 1.5-turn spiral coupler in measurement. But, considering the effect more exactly, a method of correction of line lengths is shown in Fig. 8, though this method was not tested.

Although one may make use of the meandered structure in order to reduce the overall length of a coupler, the spacing between strip conductors would necessarily be closer for the meandered case than the spiral and numerous rectangular corners would have undesired effects on the coupler performance.

V. Conclusion

In this paper, a new microwave directional coupler with a spiral-shaped construction has been described. The spiral couplers of type-*A* fabricated on alumina ceramic substrates from the design charts presented 3.5-dB maximum coupling for a 40-μm strip spacing. The spiral coupler uses much smaller area of the substrate than the conventional coupler. The calculation shows that the modified spiral coupler, type-*B*, can typically give 2.5-dB coupling for a 95-μm strip spacing on an alumina ceramic substrate of 0.635-mm thickness. We confirmed the usefulness of type-*B* coupler by trial construction on a Teflon substrate.

The method of construction of the directional coupler in this paper seems to be quite useful for obtaining a small-sized coupler with a wide band in the microwave integrated circuitry.

Appendix I
The Admittance Matrix of a 2-Turn Spiral Coupler

The admittance matrix $\tilde{Y}$ is given in (A1)

$$\tilde{Y}=\begin{bmatrix} t_{11} & t_{12} \\ t_{21} & t_{22} \end{bmatrix} \tag{A1}$$

where $t_{11},\cdots$, are given in (A2)

$$\begin{aligned} t_{11} &= u_1^{11}+(u_1^{12}+u_2^{11})w_1 \\ t_{12} &= u_2^{12}+(u_1^{12}+u_2^{11})w_2 \\ t_{21} &= u_2^{21}+(u_1^{21}+u_2^{22})w_1 \\ t_{22} &= u_1^{22}+(u_1^{21}+u_2^{22})w_2 \\ w_1 &= -(u_1^{11}+u_1^{22}+u_2^{12}+u_2^{21})^{-1}(u_1^{21}+u_2^{11}) \\ w_2 &= -(u_1^{11}+u_1^{22}+u_2^{12}+u_2^{21})^{-1}(u_1^{12}+u_2^{22}). \end{aligned} \tag{A2}$$

$u_1^{11},\cdots$, are partial matrices of u_1, u_2 in (A3)

$$u_1=\begin{bmatrix} u_1^{11} & u_1^{12} \\ u_1^{21} & u_1^{22} \end{bmatrix} \qquad u_2=\begin{bmatrix} u_2^{11} & u_2^{12} \\ u_2^{21} & u_2^{22} \end{bmatrix}. \tag{A3}$$

These matrices are derived from the admittance matrix of four coupled lines, Y, as follows:

$$u_1=x_1-\tfrac{1}{2}x_2x_1^{-1}x_2 \qquad u_2=-\tfrac{1}{2}x_2x_1^{-1}x_2 \tag{A4}$$

$$Y=\begin{bmatrix} x_1 & x_2 \\ x_2 & x_1 \end{bmatrix}. \tag{A5}$$

Matrix $Y=[Y_{ij}]$ is given in (A8).

For type-*B* coupler, the matrix Y is expressed as in (A6)

$$\tilde{Y}=s_3+s_4(A-s_1)^{-1}s_2 \tag{A6}$$

where s_1–s_4 are derived in (A7) and A is in (9c)

$$s_1=\left[\begin{array}{cc|cc} Y_{22} & Y_{23} & Y_{17} & Y_{16} \\ Y_{23} & Y_{22} & Y_{16} & Y_{17} \\ \hline Y_{17} & Y_{16} & Y_{11} & Y_{14} \\ Y_{16} & Y_{17} & Y_{14} & Y_{11} \end{array}\right]=\left[\begin{array}{c|c} s_1^{11} & s_1^{12} \\ \hline s_1^{12} & s_1^{22} \end{array}\right]$$

$$s_2=\left[\begin{array}{cc|cc} Y_{13} & Y_{12} & Y_{26} & Y_{27} \\ Y_{12} & Y_{13} & Y_{27} & Y_{26} \\ \hline Y_{15} & Y_{18} & Y_{13} & Y_{12} \\ Y_{18} & Y_{15} & Y_{12} & Y_{13} \end{array}\right]$$

$$s_3=\left[\begin{array}{c|c} s_1^{22} & s_1^{12} \\ \hline s_1^{12} & s_1^{11} \end{array}\right]$$

$$s_4=s_2. \tag{A7}$$

Appendix II
The Admittance Matrix of Four Coupled Lines (Y)

The matrix Y is expressed in (A8) in a similar manner to that described in [8]

$$\begin{aligned} &Y_{11}=Y_{44}=Y_{55}=Y_{88}=\alpha-\beta \quad Y_{14}=Y_{41}=Y_{58}=Y_{85}=\alpha+\beta \\ &Y_{12}=Y_{21}=Y_{34}=Y_{43}=Y_{56}=Y_{65}=Y_{78}=Y_{87}=\gamma-\delta \\ &Y_{13}=Y_{24}=Y_{31}=Y_{42}=Y_{57}=Y_{68}=Y_{75}=Y_{86}=\gamma+\delta \\ &Y_{15}=Y_{48}=Y_{51}=Y_{84}=\epsilon+\eta \quad Y_{18}=Y_{45}=Y_{54}=Y_{81}=\epsilon-\eta \\ &Y_{16}=Y_{25}=Y_{38}=Y_{47}=Y_{52}=Y_{61}=Y_{74}=Y_{83}=\xi+\zeta \\ &Y_{17}=Y_{28}=Y_{35}=Y_{46}=Y_{53}=Y_{64}=Y_{71}=Y_{82}=\xi-\zeta \\ &Y_{22}=Y_{33}=Y_{66}=Y_{77}=\mu+\nu \quad Y_{23}=Y_{32}=Y_{67}=Y_{76}=\mu-\nu \\ &Y_{26}=Y_{37}=Y_{62}=Y_{73}=\phi-\psi \quad Y_{27}=Y_{36}=Y_{63}=Y_{72}=\phi+\psi \end{aligned} \tag{A8}$$

where

$$\begin{aligned} &\alpha=-(r_2Y_{a1}C_1-r_1Y_{b1}C_2)/R_1 \quad \beta=(r_4Y_{c1}C_3-r_3Y_{d1}C_4)/R_3 \\ &\gamma=(Y_{a1}C_1-Y_{b1}C_2)/R_1 \quad \delta=(Y_{c1}C_3-Y_{d1}C_4)/R_3 \\ &\epsilon=(r_2Y_{a1}CS_1-r_1Y_{b1}CS_2)/R_1 \\ &\eta=(r_4Y_{c1}CS_3-r_3Y_{d1}CS_4)/R_3 \\ &\xi=-(Y_{a1}CS_1-Y_{b1}CS_2)/R_1 \quad \zeta=(Y_{c1}CS_3-Y_{d1}CS_4)/R_3 \\ &\mu=(r_1Y_{a2}C_1-r_2Y_{b2}C_2)/R_1 \quad \nu=(r_3Y_{c2}C_3-r_4Y_{d2}C_4)/R_3 \\ &\phi=-(r_1Y_{a2}CS_1-r_2Y_{b2}CS_2)/R_1 \\ &\psi=(r_3Y_{c2}CS_3-r_4Y_{d2}CS_4)/R_3. \end{aligned} \tag{A9}$$

Y_{xi} in (A9) is the normal-mode admittance of the mode x of the ith line, r_i is the element of voltage eigenvector matrix, $C_i=\coth(\gamma_i\cdot L_4)$, $CS_i=\operatorname{csch}(\gamma_i\cdot L_4)$ (L_4 is line length), $R_1=2(r_1-r_2)$ and $R_3=2(r_3-r_4)$. All these are derived from the capacitance matrix C_a and C for the vacuum- and dielectric-filled cases as follows.

$\gamma_i(i=a,b,c,d)$ are expressed in (A10).

$$\begin{aligned} &\gamma_a=j\beta\sqrt{X_1^a} \quad \gamma_b=j\beta\sqrt{X_1^b} \quad \gamma_c=j\beta\sqrt{X_2^c} \quad \gamma_d=j\beta\sqrt{X_2^d} \\ &\beta=\omega\sqrt{\epsilon_0\mu_0} \\ &X_1^a,\ X_1^b=\left(A+G+F+D\pm\sqrt{D_1}\right)/2 \\ &\qquad (+:a \text{ mode}, -:b \text{ mode}) \\ &X_2^c,\ X_2^d=\left(A-G+F-D\pm\sqrt{D_2}\right)/2 \\ &\qquad (+:c \text{ mode}, -:d \text{ mode}) \\ &D_1=(A-G-F+D)^2+4(B+C)(E+H) \\ &D_2=(A+G-F-D)^2+4(B-C)(E-H) \end{aligned} \tag{A10}$$

where A–H are the elements of the matrix $C_a^{-1}C$ as shown in (A11)

$$C_a^{-1}C=\begin{bmatrix} A & B & C & D \\ E & F & G & H \\ H & G & F & E \\ D & C & B & A \end{bmatrix}. \tag{A11}$$

$r_i(i=1,2,3,4)$ are given in (A12)

$$r_i=\begin{cases} \dfrac{(A-X_1^i)H-DE}{(F-X_1^i)D+DG-(B+C)H}, \\ \qquad i=(1,2)=(a,b) \text{ mode} \\ -\dfrac{(A-X_2^i)H-DE}{(F-X_2^i)D-DG-(B-C)H}, \\ \qquad i=(3,4)=(c,d) \text{ mode}. \end{cases} \tag{A12}$$

Finally, mode admittances $Y_{xi}(x=a,b,c,d:\ i=1,2,3,4)$ are derived in (A13)

$$\begin{aligned} &Y_{a1}=Y_{a4}=(y_{11}+r_1y_{12})/\gamma_a \\ &Y_{a2}=Y_{a3}=(y_{22}+y_{23}+y_{12}/r_1)/\gamma_a \\ &Y_{b1}=Y_{b4}=(y_{11}+r_2y_{12})/\gamma_b \\ &Y_{b2}=Y_{b3}=(y_{22}+y_{23}+y_{12}/r_2)/\gamma_b \\ &Y_{c1}=Y_{c4}=(y_{11}-r_3y_{12})/\gamma_c \\ &Y_{c2}=Y_{c3}=(y_{22}-y_{23}-y_{12}/r_3)/\gamma_c \\ &Y_{d1}=Y_{d4}=(y_{11}-r_4y_{12})/\gamma_d \\ &Y_{d2}=Y_{d3}=(y_{22}-y_{23}-y_{12}/r_4)/\gamma_d \end{aligned} \tag{A13}$$

where y_{ij} is equal to $j\omega C_{ij}(C=[C_{ij}])$.

$\lambda_{ge}/\lambda_0, \lambda_{go}/\lambda_0$ are normalized guide wavelengths for even and odd modes on the two coupled lines. These are derived from the capacitances for the vacuum (C_e^0, C_o^0) and the dielectric-filled cases (C_e, C_o) as in (A14)

$$\lambda_{ge}/\lambda_0=\sqrt{C_e^0/C_e} \qquad \lambda_{go}/\lambda_0=\sqrt{C_o^0/C_o}. \tag{A14}$$

References

[1] V. Tulaja, B. Schiek, and J. Köhler, "An interdigitated 3-dB coupler with three strips," *IEEE Trans. Microwave Theory Tech.*, vol. MTT-26, no. 9, pp. 643–645, Sept. 1978.

[2] Y. Tajima and S. Kamihashi, "Multiconductor couplers," *IEEE Trans. Microwave Theory Tech.*, vol. MTT-26, no. 10, pp. 795–801, Oct. 1978.
[3] J. Lange, "Interdigitated stripline quadrature hybrid," *IEEE Trans. Microwave Theory Tech.*, vol. MTT-17, no. 12, pp. 1150–1151, Dec. 1969.
[4] T. Itoh and A. S. Herbert, "A generalized spectral domain analysis for coupled suspended microstriplines with tuning septums," *IEEE Trans. Microwave Theory Tech.*, vol. MTT-26, no. 10, pp. 820–826, Oct. 1978.
[5] D. D. Paolino, "Design more accurate interdigitated couplers," *Microwaves*, pp. 34–38, May 1976.
[6] T. G. Bryant and J. A. Weiss, "Parameters of microstrip transmission lines and coupled pairs of microstriplines," *IEEE Trans. Microwave Theory Tech.*, vol. MTT-16, no. 12, pp. 1021–1027, Dec. 1968.
[7] G. I. Zysmann and A. K. Johnson, "Coupled transmission line networks in an inhomogeneous dielectric medium," *IEEE Trans. Microwave Theory Tech.*, vol. MTT-17, no. 10, pp. 753–759, Oct. 1969.
[8] V. K. Tripathi, "On the analysis of symmetrical three-line microstrip circuits," *IEEE Trans. Microwave Theory Tech.*, vol. MTT-25, no. 9, pp. 726–729, Sept. 1977.

Circulators Using Planar WYE Resonators

JOSEPH HELSZAJN, MEMBER, IEEE, AND W. TERENCE NISBET, MEMBER, IEEE

Abstract—**An important class of commercial three-port circulator relies for its operation on a junction resonator consisting of the symmetrical connection of three open-circuited transmission lines. A feature of this resonator is that it may be quarter-wave coupled to form a circulator with a moderate specification (25-percent bandwidth to 25-dB return loss points) and physical dimensions of the order of directly coupled conventional circulators (using a disk resonator).**

For circulators for which the in-phase eigennetwork may be represented by an ideal short-circuit, the equivalent circuit is a one-port network which may be formed from a characterization of the constituent resonator. This feature is used in this paper to study the equivalent circuit of junction circulators using planar WYE resonators. The derivation of the equivalent circuit parameters is supported with the design of a 4-GHz quarter-wave-coupled stripline circulator.

I. INTRODUCTION

AN IMPORTANT resonator with three-fold symmetry for use in the design of three-port junction circulators is the WYE resonator [1], [4]. This resonator may be coupled in either of the two ways indicated in Fig. 1(a) and (b). If it is quarter-wave coupled in the manner shown in Fig. 1(a), it may be adjusted to display the classic frequency characteristic normally associated with a quarter-wave-coupled junction circulator, but with physical dimensions of the order of a directly coupled device (using a disk resonator). The equipotential lines in such a resonator are shown in Fig. 2.

Manuscript received September 25, 1980; revised February 5, 1981.

J. Helszajn is with the Department of Electrical and Electronic Engineering, Heriot-Watt University, 31-35 Grassmarket, Edinburgh EH1 2HT, Scotland.

W. T. Nisbet is with Ferranti Ltd., Dunsinane Ave. Dundee DD2 3PN, Scotland.

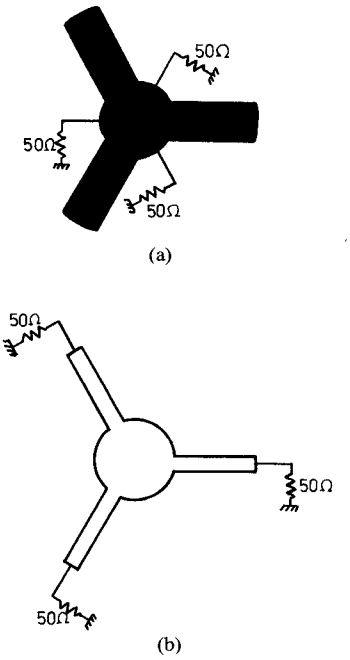

Fig. 1. Schematic diagram of circulators using planar WYE resonators. (a) High-Q connection. (b) Low Q-connection.

Circulators using planar WYE resonators have been analyzed [3] in terms of a 6×6 impedance matrix for the central nonresonant disk region, defined by the three open-circuited stubs of the resonator circuit and the coupling intervals of the circulator terminals. The boundary conditions at the terminals of the three stubs are subsequently

0018-9480/81/0700-0689$00.75